Cinnamaldehyde hydrogenation with bimetallic AuPd catalysts

S. Cattaneo[a,*], N. Dimitratos[a], S. J. Freakley[a], D. Morgan[a], M. Sankar[a] and G. J. Hutchings[a,*]

[a] *Cardiff Catalysis Institute, School of Chemistry, Cardiff University, Cardiff, CF10 3AT, United Kingdom.*
*CattaneoS@cardiff.ac.uk; Hutch@cardiff.ac.uk

The hydrogenation of cinnamaldehyde was studied over a series of bimetallic AuPd supported catalysts with different Au/Pd ratio and their performances in terms of activity and selectivity compared with the monometallic Au and Pd. Of all the catalysts studied, Au50Pd50/TiO2 (Au/Pd (1/1 molar ratio), was found to be the most active, while the monometallic Pd/TiO_2 the most selective towards hydrocinnamaldehyde. A first systematic study on the impact of reaction parameters, such as stirring speed, catalyst amount, hydrogen pressure and reaction temperature, was conducted and the effect of different solvents and supports was also studied. All the catalysts have been fully characterised by UV-VIS, DLS, MP-AES, HRTEM, XPS, XRD, DRIFT and FTIR; in particular, analysis of the used catalyst using FTIR, showed the presence of adsorbed carbonyl surface products, that coupled with Pd leaching, is the main reason of catalyst deactivation.

1. Introduction

Supported metal nanoparticles are widely used in catalysis for a broad range of selective reactions. Gold nanoparticles, in particular, since Haruta[1] and Hutchings[2] disclosed the peculiar activity of this metal in CO oxidation and ethylene hydrochlorination 20 years ago, have been extensively used in numerous redox reactions such as hydrogenations of nitro compounds,[3] selective oxidations of alkenes to epoxides[4,5] and alcohols to aldehydes,[6] and many other chemical synthesis.[7–10] The history of palladium as a catalyst is far older and date back to the nineteenth century when Graham discovered its outstanding ability to absorb hydrogen compared to any other metal, and later with the first studies on reactions catalysed by palladium blacks.[11] Nowadays palladium is largely used in heterogeneous catalysis in several reactions, such as selective alcohol oxidations,[12–14] unsaturated hydrocarbon hydrogenations,[15,16] and the lately discovered C-C coupling reactions.[17–19] More recently, it has been shown that alloying palladium with gold can enhance the activity of the catalyst for particular reactions including the oxidation of benzyl alcohol[20] and the direct synthesis of hydrogen peroxide.[21,22]

α,β-unsaturated aldehydes are very important molecules in the industrial synthesis of pharmaceuticals, fragrances and fine chemicals.[23–26] With an estimated production of 1500 ton/a via a base-catalysed condensation of benzaldehyde and acetaldehyde,[27] cinnamaldehyde (CAL) is one of the most significant fragrance aldehydes and therefore plays a key role in this sector; in addition to its use in perfumery, it is used also as polymerisation and corrosion inhibitor and for the coating of metals.[28] The selective hydrogenation of the vinyl (C=C) or carbonyl (C=O) group, leads to hydrocinnamaldehyde (HCAL) and cinnamyl alcohol (COH) respectively, that are reported to be used as intermediates in HIV pharmaceuticals and in perfumery.[27,29] Further hydrogenation, results in hydrocinnamyl alcohol (HCOH) and phenyl propane (PPR) by hydrogenolysis mechanism (Figure 1). Currently, several transition and noble metal based catalysts are reported in literature to be active in the hydrogenation of cinnamaldehyde.[24] Au, for example, requires usually harsh reaction conditions to obtain good conversion and it generally selectively hydrogenate the carbonyl group leading to the formation of COH. *Bus et al.,* reported for example the conversion of CAL with Au/γ-Al_2O_3 to COH with a selectivity up to 90 % at 85 bar of H_2 and 100 °C. In their studies, high selectivity to COH were produced from the initial stages of the reaction, and the selectivity remained unaltered up to 85 % of conversion, after which all the COH further convert into HCOH.[30] Similar results were obtained by other research groups with different supports such as CeO_2,[31] SiO_2[32] and α-Fe_2O_3,[33] while CNT and Zr_2O_3 promoted the hydrogenation of the vinyl group.[32,34] Interestingly, Milone and co-workers, found high activity towards cinnamyl ethyl ethers when Au was supported onto TiO_2 and used in alcohol solvents.[35] On the other hand, Pd nanoparticles are reported to be more selective towards the hydrogenation of the C=C bond both when supported[23,36–38] or when stabilised in ionic liquids.[39]

A plethora of studies on different supports, solvents and hydrogen sources have been reported in literature.[30–34,40–42] However, very few articles have been focused the attention on the catalytic performance of AuPd bimetallic catalysts. *Dash et al.,* reported equimolar production of HCAL and HCOH using bimetallic nanoparticles stabilised in imidazolium ionic liquids when the Au/Pd molar ratio was 3:1 and 1:3, while an enhancement in HCOH was observed when the two metals were present in the same molar amount.[43] Similar results were obtained by Szumelda and co-workers using AuPd/C catalysts prepared by reverse water-in-oil microemulsion method.[44] On the other hand, *Parvulescu et al.* observed an increase in COH production using AuPd colloids embedded in SiO_2,[45] although not much importance was given to the alloy composition and the reaction optimisation, since their report was more focused on general hydrogenation reactions. Very high selectivity towards HCAL was obtained by *Yang et al.* with bimetallic nanoparticles supported on mesoporous SiO_2.[46] A different approach to obtain HCAL in high selectivity was studied by Gu and co-workers:[47] separate deposition of Au and Pd nanoparticles was achieved onto ordered mesoporous carbon, and the authors ascribed the superior activity to the

better H_2 dissociation properties of the Pd nanoparticles, while Au nanoparticles suppressed the deep hydrogenation process acting as hydrogen acceptors and diluting the Pd active sites. Severe sintering and aggregation phenomena were however observed during the heat treatments these catalysts undergone (NPs size varied from 2.3 ± 0.5 to 15 ± 5 nm), thus making difficult any comparison in term of activity.
In the present work, preformed colloidal AuPd nanoparticles with narrow size distribution were prepared via a sol-immobilisation method, a facile and green technique that allows a better control over nanoparticles size/shape and particle dimension. These preformed nanoparticles were then immobilised onto different supports and tested in the selective hydrogenation of cinnamaldehyde under mild conditions. The influence of variables such as stirring rate and catalyst amount (substrate to metal molar ratio) has been studied from an experimental point of view in order to assure a chemically-controlled regime in the working conditions. Finally, the effect of reaction temperature, hydrogen partial pressure, support, solvent and Au/Pd molar ratio has been analysed in terms of activity and selectivity to desired products, and multiple reusability runs have been performed to evaluate the reusability and stability of the catalyst.

2. Experimental

2.1 Materials

$HAuCl_4$ and $PdCl_2$ were purchased from Sigma-Aldrich (99.999 % purity) and used as metal precursors. Commercial TiO_2 (Degussa, P25), MgO (Fisher Scientific, light) and activated carbon (Sigma-Aldrich, DARCO G60) were used as supports, while for the Fe_2O_3 preparation, Na_2CO_3 (Sigma-Aldrich, 99.9 %) and $Fe(NO_3)_2$ x 9 H_2O (Sigma-Aldrich, 98 %) were employed. $NaBH_4$ (granular, 99.99 % purity) and polyvinyl alcohol (PVA, Mw = 9,000-10,000, 80 % hydrolyzed) from Sigma-Aldrich were used for the catalysts preparation. Cinnamaldehyde (Sigma-Aldrich, 99 %), cinnamyl alcohol (Alfa Aesar, 95 %), hydrocinnamaldehyde (Sigma-Aldrich, 98 %), hydrocinnamyl alcohol (Sigma-Aldrich, 98%) and phenylpropane (Sigma-Aldrich, 98 %) were used as substrates and/or as standards for quantification analysis. Toluene (Sigma-Aldrich, > 99 %), ethanol (VWR, 99.8 %) and 2-propanol (Sigma-Aldrich, 99.5 %) were employed as solvents.

2.2 Catalyst preparation

The α-Fe_2O_3 support was prepared by co-precipitation of $Fe(NO_3)_2$ x $9H_2O$ and Na_2CO_3.[28] In a standard 10 g preparation methodology, 48 g of $Fe(NO_3)_2$ were dissolved in 500 mL of hot water and the solution was added to 435 mL solution of Na_2CO_3 (23 g) maintained at 80 °C under vigorous stirring. After 1 hour, the precipitate was filtered, washed with hot water, dried at 110 °C overnight and calcined for 3 hours in static air at 300 °C using a heating rate of 10 °C/min.
All the Au, Pd and AuPd catalysts here reported were prepared by sol-immobilisation method as follows: To an aqueous solution of $HAuCl_4$ and/or $PdCl_2$ of the desired concentration (total metal concentration 0.127, 0.130, 0.143, 0.165, 0.194, and 0.235 mmol/L for Au/Pd molar ratios of 100:0, 95:5, 75:25, 50:50, 25:75 and 0:100 respectively), the required amount of a PVA solution (1 wt %) was added (PVA/(Au + Pd) (w/w) = 1.2 for bimetallic catalysts, 0.65 for monometallic catalysts). A freshly prepared solution of $NaBH_4$ (0.1 M, $NaBH_4$/(Au + Pd) (mol/mol) = 5) was then added to form a ruby-red sol when monometallic gold was prepared or a dark-brown sol when AuPd or Pd sols were prepared. After 30 minutes of sol generation, the colloid was immobilised by adding the desired support and acidified at pH 1 by sulfuric acid (except for MgO, where no acidification is required) under vigorous stirring. The amount of support material required was calculated so as to have a total final metal loading of 1 wt. %, and the molar ratio of Au/Pd was varied by adjusting the relative concentrations of the metals in aqueous solution. After 1 h, the slurry was filtered and the catalyst was washed thoroughly with 2 L of distilled water and dried at 120 °C for 16 h. This method allows a better control of the size, shape and structure of nanoparticles.[48]
High temperature treatments were performed where specified on the $Au_{50}Pd_{50}/TiO_2$ catalyst as follows. The dried catalyst was first calcined in static air for 4 hours at either 200, 300 or 400 °C with a heating ramp of 10 °C/min and finally reduced at the same calcination temperature under a 5 % H_2/Ar flow for another 4 hours.

2.3 Catalyst evaluation

The hydrogenation of cinnamaldehyde was used as a hydrogenation model reaction. The hydrogenation reactions were carried out in a Radleys carousel reactor using 5 parallel 50 mL glass reactors stirred using magnetic bars. In a typical reaction, the requisite amounts of catalyst (50 mg, typical substrate/metal molar ratio 1200:1), substrate (500 µL, 4 mmol) and solvent (5 mL of toluene, ethanol or 2-propanol) were charged into the reactors at room temperature which were then purged with H_2 (3 times) before the reactors were sealed using Teflon screw threaded caps. The reactors were always connected in parallel to the gas-line to ensure the consumed gas was replenished and the pressure was monitored by a pressure gauge fitted in the inlet line. The reactors with the reaction mixture were loaded into a preheated heating block, which was maintained at the desired reaction temperature and pressure (typical 100 °C and 1 H_2 bar). The reaction started by commencing stirring inside the reactors at 1000 rpm. After reaching the desired amount of time, the reactors were taken out the carousel and cooled down in an ice bath for a period of 5 minutes to quench the reaction. The content of the

reactors was centrifuged and an aliquot of the supernatant reaction mixture (0.5 mL) was diluted with a solution of external standard (0.5 mL of a 0.7 M solution of o-xylene in the appropriate solvent) for GC measurement. For the analysis of the products, a GC-MS (Shimadzu, GCMS-QP2010SE) was employed and the resulting fragmentation peaks compared with standards present in the software database, while for the quantification of the amounts of reactants consumed and products generated, a GC-FID (Agilent 7820A equipped with an Agilent HP-5, 30 m x 320 µm x 0.25 µm column) was employed and the external calibration method was used.
The catalyst reusability was carried out using the following experimental procedure. The reaction was carried out in the batch reactor as described above. After 90 minutes the flask was cooled down in an ice bath and the catalyst was left decanted in order to separate and remove the reaction mixture from the catalyst. The used catalyst was then washed either with acetone or with toluene, left decanted for 6 hours and the washing solvent was removed from the reactor. A second reaction was then started with the washed catalyst and this procedure was repeated for a total of 4 runs.
The cinnamaldehyde conversion, product selectivities and TOF were calculated according to the following definitions:

$$CAL\ Conversion\ (\%) = \frac{C_0 - C_t}{C_0} * 100$$

$$Selectivity_{i,t}\ (\%) = \frac{C_{i,t}}{C_{CAL\ 0} - C_{CAL\ t}} * 100$$

$$TOF\ (h^{-1}) = \frac{moles_{CAL\ converted}}{moles_{Metals} * t}$$

2.4 Material characterisation

The metal colloids were analysed by dynamic light scattering (DLS, Malvern Zetasizer Nano ZS) and UV-vis (Agilent Cary 60) techniques to determine the hydrodynamic diameter of the metal nanoparticles in a liquid environment and the presence or absence, position and intensity of the surface plasmon resonance peak of gold and completion of metal precursor reduction, respectively. Both DLS and UV-vis spectra were recorded in disposable polystyrene cuvettes after 30 minutes of sol generation.
TEM experiments were carried out on a JEOL JEM-2100 electron microscope with a 200 kV accelerating voltage. The samples were first dispersed in methanol and sonicated for 5 minutes and then a drop was placed onto a 300 mesh carbon-coated copper grid.
XRD measurements were carried out at room temperature with a PANalytical X'PertPRO using a Cu Kα radiation source, (Kα, λ= 1.5418A). The complete diffractograms were collected over the 10-80 ° 2θ range at a rate of 1 °/min. The metal loading of the catalysts was verified using an Agilent 4100 MP-AES. The samples were firstly dissolved in aqua regia, diluted and filtered to remove the undissolved support.
X-ray photoelectron spectroscopy (XPS) measurements were performed on a Thermo Scientific K-alpha+ spectrometer. Samples were analysed using a monochromatic Al x-ray source operating at 72 W (6 mA x 12 kV), with the signal averaged over an oval-shaped area of approximately 600 x 400 microns. Data was recorded at pass energies of 150 eV for survey scans and 40 eV for high resolution scan with a 1eV and 0.1 eV step size respectively. Charge neutralisation of the sample was achieved using a combination of both low energy electrons and argon ions (less than 1 eV) which gave a C(1s) binding energy of 284.8 eV. All data were analysed using CasaXPS (v2.3.17 PR1.1) using Scofield sensitivity factors and an energy exponent of -0.6.
Diffuse reflection infrared spectroscopy (DRIFT) was carried out with a Bruker Tensor 27 spectrometer fitted with a HgCdTe (MCT) detector and operated with OPUS software. The Harrick Praying Mantis HVC-DRP-4 cell was equipped with ZnSe windows and included gas inlet and outlet and vacuum ports as well as capabilities for heating and cooling. For CO adsorption studies, the required gas flow was introduced using a 2 % CO/N_2 gas mixture at 40 $cm^3\ min^{-1}$ of, over a period of x seconds or minutes. The mixture composition and flow rate was controlled by mass-flow controllers. Each absorbance spectrum represents an average of 64 scans with a spectral resolution of 2 cm^{-1}. Prior to analysis, the gas-phase CO signal was removed by subtracting the spectra recorded under CO containing atmosphere, followed by background and normalisation of the spectra. No high temperature pretreatments were performed on the catalysts in order to preserve eventual very small metal clusters that may undergo sintering at elevated temperature. When pyridine was employed as probe molecule, a 60 $cm^3\ min^{-1}$ flow of N_2 was bubbled into a sealed flask containing pure pyridine and successively into the cell mantained at a constant temperature of 30 °C. After 15 minutes, the gas flow was switched off while opening the vacuum line, and the analysis started. The temperature was gradually increased by 50 °C consecutive steps up to 480 °C and mantained for 15 minutes, at the end of wich, spectra were collected. As for the CO spectra, each absorbance spectrum rapresented an average of 64 scans with a spectral resolution of 2 cm^{-1}. All the samples were previously pretreated at 150 °C under static air for 1 h in order to remove all the adsorbed H_2O. Background and normalisation of the spectra were performed on dehydrated KBr.

3. Results and discussion

3.1 Catalyst characterisation

Catalyst metal loading and Au/Pd ratios obtained by MP-AES and XPS are in good agreement with the nominal values (1 wt. %) and the results are reported in the Supporting Information (Table S1).

TEM and DLS analysis were performed to determine the average particle size and particle size distribution (Figure 2 and Table S2). Representative bright field TEM micrographs as shown in Figure 2, were acquired to measure the particle size distributions and mean particle sizes of the supported Au_xPd_y nanoparticles. The particle size data are summarized in Table S2. The mean particle sizes of the supported Au_xPd_y nanoparticles were in the 2.1 (±0.4) -2.7 (± 1.0) range without observing any appreciable systematic size trend with variation of Au_xPd_y atomic composition. The average diameter of Au_xPd_y colloids using DLS was in the range 4-7 nm. Since the DLS measures the hydrodynamic diameter, the PVA layer and the water solvation shell that surrounds the colloidal nanoparticles are responsible of the differences in the order of 2.5-5.0 nm compared to TEM analysis. The presence of small nanoparticles was also confirmed by XRD analysis (Figure S2). Scherrer equation couldn't be applied for the calculation of the crystallite size due to the small signal to noise ratio caused by the very low intensity of Au (200) and Pd (200) diffraction peaks. XRD analysis were performed also on the $Au_{50}Pd_{50}$/MgO catalyst to verify the actual composition of the support (Figure S3). As expected, since the catalyst wasn't calcined at high temperature, the support presents the characteristic (001), (101), (102) and (110) peaks (at 19, 38, 51 and 59 ° respectively) of the $Mg(OH)_2$ brucite phase.[49–51]

XPS analysis of the monometallic and bimetallic catalysts are shown in Figure 3. For the whole series of samples, the Au(4f) spectra showed the presence of Au in metallic state and the values of the binding energy (BE) of the $Au4f_{7/2}$ peak were in the 83.3-83.7 eV range in agreement with previous reports.[48] The Pd(3d) spectra showed the presence of of metallic Pd (334.9 eV) as the major species and Pd^{2+}, attributed mainly to PdO (337.0 eV), (Figure 3b). For the monometallic Au/TiO_2 sample the BE of Au was 83.7 eV, lower than the typical value obtained for the bulk gold (ca. 84.0-84.2 eV). The slight decrease to lower BE could be attributed to (i) particle size effect and (ii) charging of Au particles (presence of Au with partially negative charge $Au^{\delta-}$). The addition of Pd to the Au samples caused a downward shift in the BE of Au from 83.7 to 83.3 eV which indicates a possible electronic interaction between the Au and Pd as noted by Lee *et al*.,[52] in common with that study the Pd BE shifts were no greater than 0.2 eV, which we consider to be the experimental confidence limit for absolute BE (Figure S4). Moreover, XPS analysis for the bimetallic catalysts showed that the Pd/Au atomic ratios were close to the expected nominal values suggesting the presence of random alloys rather than core-shell structures and in agreement with our previous reports (Table S1).

CO-DRIFT analysis were performed on the bimetallic Au-Pd and monometallic Au, Pd catalysts. The results are reported in Figure 4. The monometallic Au catalyst (Figure S6) shows a primary peak at around 2120 cm^{-1} comprised by two peaks at 2124 and 2112 cm^{-1} and assigned according to previous reports to CO linearly bonded on Au^0 step sites on top of nanoparticles and on peripheral Au^0 step sites respectively.[53,54] The presence of the latter peak, in particular, confirm the presence of very small nanoparticles on the catalyst surface. The peak at 2072 cm^{-1}, on the other hand, has been assigned to linear CO adsorbed on $Au^{\delta-}$ species.[55] These partially negative species seems to form during the gradual reduction of Au^0 to $Au^{\delta-}$ by the adsorbed CO[56], as shown by analysis at early stage of CO adsorption (Figure S6, however from XPS analysis we cannot exclude the presence of a small portion of Au $^{\delta-}$species; the better stability of partially negative Au atoms has been ascribed to the greater π-back-donation of the latter species.[57] The broad peak at 2050-1950 cm^{-1} has been assigned to bridge bonded CO on $Au^{\delta-}$ species. The presence of this broad band is a direct effect of very well dispersed small Au nanoparticles on the surface of support. As reported by *Tabakova et al*., this band indicates isolated sites not interacting with each other, and thus the bond between the CO and the site is altered as a consequence of an electron transfer from the support to the metal;[58] this results were recently confirmed by DFT studies.[59]

The monometallic Pd catalyst (Figure S7), presents two broad group of peaks. The first group, is comprised by 3 peaks at 2130, 2096 and 2083 cm^{-1}; the latter two peaks have been assigned to linear CO coordinated on Pd^0,[60–62] while the peak at 2130 cm^{-1} indicates the presence of Pd^+ species.[61,62] These positive charged Pd species are not present originally in the catalyst, as confirmed by XPS analysis, but are most likely the result of partial reduction of Pd^{2+} species by the coordinated CO molecules. The second group at lower wavenumbers, is comprised by multiple and broad peaks assigned to μ_2 bridge bonded CO (ca. 1980-1930 cm^{-1}) and μ_3 bridge bonded CO (ca. 1930-1820 cm^{-1}) in accordance with previous literature.[60,62]

Regarding bimetallic AuPd catalysts, it has been previously reported that Pd carbonyls are much more stable than Au carbonyls due to the higher π-back-donation of the Pd-CO bond.[63] For this reason, the typical Pd-CO bands dominate the DRIFT spectra in AuPd alloys when Pd is present in significant amount and it is therefore difficult to observe bands related to the presence of Au sites. Indeed, in the $Au_{35}Pd_{65}$, $Au_{50}Pd_{50}$ and $Au_{65}Pd_{35}$ catalysts, all the CO-Pd features listed above for the monometallic Pd catalyst are present,[64] and the only difference among these catalysts is the intensity of the peaks: as expected, increasing the amount of Pd, the intensity of the CO-Pd peaks increases (Figure S8). The smaller intensity of the linear CO-Pd in the monometallic catalyst compared to the $Au_{35}Pd_{65}$ and $Au_{50}Pd_{50}$, can be explained by the presence of bigger nanoparticles (2.7 ± 1.0 nm, 2.3 ± 0.8 nm and 2.1 ± 0.6 nm respectively). This is also confirmed by the presence of peaks in the 1980-1820 cm^{-1} region characteristic of μ_2 and μ_3 bridge bonded CO with Pd that can only be formed on

relatively bigger nanoparticles. The same explanation applies to the $Au_{65}Pd_{35}$ catalyst, where the nanoparticle mean size is very similar to the Pd/TiO_2. Interestingly, when the Au/Pd ratio is 95:5, the CO stretching are dominated by the CO-Au interactions (Figure S9). The appearance of a strong peak at 2123 cm^{-1} with a small shoulder at 2103 cm^{-1} is evident and these peaks are characteristic of linear CO bonded on Au^0 step sites on top of nanoparticles and of peripheral Au^0 step sites, as previously discussed.

Pyridine-DRIFT was used to evaluate the presence of Lewis and Brønsted sites on bimetallic AuPd catalysts on different supports. Figure 5 shows the comparison between the spectra of $Au_{50}Pd_{50}$ nanoparticles supported on carbon, titanium oxide, iron oxide and magnesium oxide in vacuum at 30 °C after 15 minutes of saturation in a pyridine/N_2 atmosphere. It should be firstly pointed out that the MgO spectra in pure N_2 (Figure S10), show the characteristic features of $Mg(OH)_2$; this is not surprising, since no calcination has been performed on the catalyst. In particular, the peaks at 3706 and 3736 cm^{-1} are single *v*OH of $Mg(OH)_2$ and isolated OH group respectively, while the broad peak at 3600-3000 cm^{-1} is assigned to the presence of adsorbed H_2O and hydrogen bound hydroxyl groups.[65] Both carbon and magnesium oxide show two peaks of small intensity at 1590 and 1440 cm^{-1} relative to liquid-like pyridine[65,66]. These peaks deplete by increasing the temperature up to 80 °C. No other peaks relative to Lewis or Brønsted sites were detected. Titanium oxide and iron oxide, on the other hand, show interesting peaks. The former, in particular, shows strong peaks at 1603, 1573, 1494 and 1444 cm^{-1} characteristic of acid Lewis species.[67,68] These peaks are very stable to high temperature outgassing (Figure S11) and are indicative of coordinatively unsaturated metal sites on the surface of the support, as reported by Zaki et al.[68] In the same study, the authors ascribed the small peak at 1594 cm^{-1} to H-bonded pyridine molecules, thus indicating the availability of H-bond donor sites on the TiO_2 surface. Finally, the peaks at 1640 and 1545 cm^{-1} are Brønsted acid sites;[68–70] in this case, as per the H-bond sites, the peaks are not stable at high temperature outgassing (Figure S10). No basic sites or acid-base pair sites are present on the catalyst surface, as confirmed by the absence of α-pyridone and O^{2-} sites peaks, at 1680-1650 and 1260-1250 cm^{-1} respectively.[68] Regarding the Fe_2O_3 catalyst, the 4 main peaks at 1592, 1581, 1482 and 1438 cm^{-1} can be assigned to acid Lewis species.[71] Every main peak, however, has at least one shoulder that may be ascribed to slightly different acidic sites, according to a previous report.[67] The Lewis acid peaks, in particular, are divided in 4 main groups as follow: (a) 1602 and 1592 cm^{-1}, (b) 1581 and 1576, (c) 1489 and 1482 cm^{-1} and (d) 1443 and 1438 cm^{-1}. Increasing the outgassing temperature, only the strongest Lewis acid sites are able to coordinate with the CO, and thus is easier to identify the 4 main peaks at 1602, 1576, 1489 and 1443 cm^{-1} (Figure S12).

3.2 Optimisation of cinnamaldehyde hydrogenation reaction conditions with $Au_{50}Pd_{50}/TiO_2$

Cinnamaldehyde (CAL) hydrogenation reactions were initially performed at 100 °C and under 1 bar of H_2 using a bimetallic gold-palladium catalyst ($Au_{50}Pd_{50}/TiO_2$, 1 wt.%, 1:1 Au/Pd molar ratio) as our chosen model catalyst, and the main products observed were cinnamyl alcohol (COH), hydrocinnamaldehyde (HCAL), hydrocinnamyl alcohol (HCOH) and phenylpropane (PPR).

The conditions to avoid diffusion limitations and identify kinetic regime were carried out. The stirring rate effect was studied in the range of 250 and 1250 rpm, maintaining all the other parameters constant as follows: T = 100 °C, P_{H2} = 1 bar, catalyst amount = 50 mg, CAL = 4 mmol, CAL/Metal molar ratio = 1200:1, toluene = 5 mL, reaction time = 30 – 150 min. In Figure 6a are reported the performance of the catalyst at various stirring rates in terms of activity expressed as turnover frequency numbers (TOF). The results showed no mass transfer limitations in the rage 750-1250 rpm, while a further decrease in the stirring rate leads to a decrease in hydrogenation activity. Fittings these data separately, results in the identification of two regimes (presented as two straight lines) intersecting at around 550 rpm; this value can be considered as the minimum stirring speed necessary in order to avoid any diffusion limitations.

The substrate to metal ratio was then varied between 800 and 6000 (mol/mol) using stirring speed of 1000 rpm in order to study the effect of the catalyst amount (substrate to metal molar ratio). In practical terms, the amount of catalyst was varied between 10 to 70 mg. Changes in substrate/metal molar ratios in the chosen range seem to not affect the activity in terms of TOF (Figure 6b); indeed, the conversion follows a linear increase or decrease as the catalyst amount was varied. Therefore, for the chosen catalyst amount range, no mass transfer limitations were present and the reactions were thus performed in a chemically controlled regime. For both stirring speed and catalyst amount, any variation led solely to changes in activity, while the selectivity calculated at 30 % iso-conversion remained always constant (Figure S13 a and b); HCAL and HCOH were the two main products and produced in comparable amount (42 – 46 %) while the selectivity towards the unsaturated alcohol COH remained constant at 15 %. Only traces of PPR were found at these reaction conditions (< 2 %).

The influence of hydrogen pressure on both activity and selectivity was also analysed. Several experiments were carried out varying the hydrogen pressure from 1 to 3 bar and using the optimised reaction conditions reported above. Higher value of hydrogen pressure could not be investigated due to reactor pressure limitations. The increase of H_2 pressure enhances the solubility of the gas into the reaction medium, increasing the accessibility of H_2 molecule. Figure 6c shows that the TOF for cinnamaldehyde hydrogenation increased linearly from 600 to 1080 h^{-1} as the partial pressure increased in the studied range, confirming that the reaction is a first order in respect of the hydrogen partial pressure.[46] The reaction temperature effect was subsequently evaluated by varying the reaction temperature from 40 to 100 °C and maintaining the hydrogen partial pressure constant at 1 bar. It is well known that hydrogenation rates usually increase with increasing temperatures,[72] and indeed, as expected, decreasing the temperature, the TOF decreased linearly as shown in Figure 6d. It should be noted, however, that the hydrogenation selectivity to HCAL at iso-conversion

level over the $Au_{50}Pd_{50}/TiO_2$ catalyst remained unchanged with variation of both H_2 pressure and reaction temperature (Figure S13 c and d, 40 – 45 % selectivity at 30 % of iso-conversion). This behaviour is in agreement with previous studies on bimetallic catalysts.[46,73,74]

The apparent activation energy was calculated from Arrhenius plot and the value was 24 KJ mol^{-1} (Figure S14). The obtained value is in good agreement with the data reported in the literature for various metal based catalysts (Table 1).[23,74–77]

3.3 Mechanistic considerations

The simultaneous presence of both a carbonyl and vinyl group in the substrate, induces the cinnamaldehyde hydrogenation reaction as an ideal reaction for tuning and controlling the selective hydrogenation of specific functional groups. Several experimental parameters play a critical role for directing selectivity, and particularly the metal composition and support used. Using the optimised conditions presented above (100 °C, 1 bar of H_2, 1000 rpm, 50 mg of catalyst, 4 mmol of CAL and 5 mL of toluene), the CAL was converted in less than 3 hours, and the main product was the fully hydrogenated HCOH. Time on line profile (Figure 7) showed that high selectivity to HCAL are produced at the initial stage of the reaction (40 % selectivity after 30 minutes), while only traces of COH and PPR can be found respectively at the beginning and at the end of the reaction. To elucidate the possible reaction pathways, reactions were carried out using HCAL and COH intermediates as substrates (Table 2). When HCAL was employed as starting material, in fact, no products were formed after 30 minutes, while 100 % conversion was reached using COH, with a selectivity of 92 % towards the HCOH and the presence of PPR as minor product (8% selectivity). These results suggest the presence of a minor hydrogenolysis mechanism of the OH group in the COH molecule due to the minor production of PPR, since after only 30 minutes the selectivity towards PPR is much higher than using CAL as substrate.

Based on these results and taking into account previous reported data, the following proposed mechanism of reaction is presented in Figure 8. It has been reported that the adsorption of cinnamaldehyde onto the surface of the catalyst is favoured by the intrinsic planar conformation of the aromatic aldehyde;[40,44] this allows a strong interaction between the aromatic ring and the C=C and C=O double bonds. However, as soon as the C=C functional group is hydrogenated, the cinnamaldehyde assume a more three-dimensional structure, that does not allow the simultaneous interaction of the aromatic ring and the C=O unsaturation with the active sites. On the other hand, the hydrogenation of the carbonyl group only slightly changes the 3D structure of the molecule, and thus a strong interaction remains. This mechanism is also confirmed by the results of the reactions performed.

3.4 Solvent effect

Toluene was initially employed as solvent in order to avoid potential transfer hydrogenations of CAL with hydrogen releasing solvents. Different polar solvents were then tested to evaluate the efficiency in terms of catalytic performance for the hydrogenation reaction. It has been shown previously that the solvent plays a very important role in this reaction in terms of activity and selectivity. For this reason, ethanol and isopropanol, the most used solvents in literature for this reaction,[30,33,40,44,45] were employed maintaining all the other experimental parameters constant. It has been reported for the CAL hydrogenation reaction over Pd/C, Pt/C and Co/Al_2O_3, that polar solvents activate the hydrogenation of the carbonyl group, while non-polar solvents favour the hydrogenation of the vinyl group.[78] Our results (Figure 9) show an apparent small variation of catalytic activity (a variation of only ± 7 % conversion after 2 hours), while the selectivity was significantly varied. It is interesting in particular to notice the strong decrease in selectivity to HCAL, especially with ethanol (only 3 % is produced at 85 % conversion), and the increase of PPR in term of selectivity (from 3 % with toluene up to 18 % with ethanol). Moreover, it has been reported in literature the formation of acetals in presence of acid Lewis sites and small chain alcohols for this reaction,[33,45] and indeed higher amounts of acetals were produced both with ethanol and isopropanol as the chosen solvents (33 % and 25 % respectively); due to the low production of HCAL in ethanol, only the acetal derived from the interaction between one molecule of CAL with two molecules of solvent was produced, whereas in isopropanol the HCAL acetal was also present.

3.5 Support effect

It has been reported that the presence of basic OH sites improves the activity and selectivity in some hydrogenation reactions.[79] Therefore, a range of four different supports with different acid properties were studied (Table S3), namely titanium oxide, iron oxide, magnesium oxide (magnesium hydroxide, as confirmed by DRIFT analysis) and activated carbon (Figure 10). However, contrary of what reported by *Zhang et al.,* in our study we observed a decrease in catalytic activity when $Mg(OH)_2$ was employed. TiO_2, in fact, resulted the most active catalyst among the one studied, with a TOF of 769 h^{-1}, while when active carbon was employed, the activity reduced by half (TOF of 385 h^{-1}). Both Fe_2O_3 and MgO show very low activity, with a TOF of only 98 and 180 h^{-1} respectively. Using the results obtained with the pyridine-DRIFT setup, we tried to correlate the catalytic data to the Lewis/Brønsted acidity properties of the different supports. As discussed before, both TiO_2 and α-Fe_2O_3 have acid sites, however only the former has high activity towards the hydrogenation reaction, while the the latter resulted the less active among the supports studied. For this reason, it's hard to draw any correlation between

activity and Lewis/Brønsted acidity. From a selectivity point of view, the less active Fe_2O_3 and MgO appear to be the most selective towards HCAL formation, with a selectivity of almost 80 % compared to 61 and 42 % with carbon and TiO_2 respectively. Metal oxides such as Al_2O_3 and SiO_2, have proven to enhance the selectivity towards saturated aldehydes in previous studies.[80–82] When compared to activated carbon, this enhancement was explained by a better metal dispersion and to the presence of partially oxidised metal species.[83] Moreover, reducible metal oxides such as TiO_2 and Fe_2O_3, have been used for the selective hydrogenation of carbonyl group in α,β-unsaturated aldehydes; this enhancement in selectivity was generally explained as consequence of strong metal support interaction (SMSI) and as modification of the electronic properties of the metal by Fe sites specifically for iron oxide supports.[82,84–86] In our case, however, the catalysts were not undergone high temperature treatments, and the significant production of HCOH when TiO_2 was used cannot be related to SMSI effect. It has however been proposed that Lewis acid sites improve the interaction between the support and the carbonyl group, thus increasing the hydrogenation rate of the C=O bond.[87] This can explain the presence of high selectivity towards the HCOH in the reaction mixture when titanium oxide was employed. It worth also notice the PPR increase in selectivity when activated carbon was employed, possibly due to its highly-functionalised surface. This is not unexpected, since activated carbon is known to enhance the hydrogenolysis mechanism.[88] Different group functionalisation may be also responsible for the general a specific selectivity of the carbon catalyst towards the hydrogenation of either the vinyl or the carbonyl group.

3.6 Au/Pd ratio effect

The effect of Au/Pd molar ratio was studied in order to understand the role and impact of Au to affect (i) the activity of cinnamaldehyde (adsorption of cinnamaldehyde on metal active sites) and (ii) tune the selectivity towards to the C=O or C=C hydrogenation. TiO_2 was used as support because due to the relative low selectivity towards a specific product, it's easier to detect changes in selectivity. A series of catalysts with different Au/Pd metal molar ratios were prepared (Au, $Au_{95}Pd_5$, $Au_{65}Pd_{35}$, $Au_{50}Pd_{50}$, $Au_{35}Pd_{65}$, and Pd, Table S1). Monometallic Au/TiO_2 and $Au_{95}Pd_5$/TiO_2 catalysts were completely inactive (Figure 11); an increase of catalytic activity based on TOF was observed only with a further addition of Pd, meaning that a minimum amount of this noble metal is required to initiate the reaction. This is in agreement with the CO-DRIFT results (Figure 4), where no Pd features were detected in the $Au_{95}Pd_5$ catalyst. When the molar ratio between Au and Pd is approximately 50:50, the activity reached a maximum with a TOF of 836 h^{-1}, and a further addition of Pd decreased the catalytic performance. Activity enhancement due to alloying effect were also reported by other groups, but no effect on selectivity was reported.[43,46] ^{43,46}^{43,46}^{43,46}^{43,46}Only *Parvulescu et al.,* reported an increase in COH selectivity using AuPd colloid embedded in SiO_2 as catalyst,[45] while Szumelda and co-workers observed a progressive decrease in both activity and selectivity towards HCAL starting from a Pd/C catalyst and increasing the amount of Au.[44] In both cases, changes in selectivity are explained as geometrical and electronical effects. It is clear from these results that Au, although totally inactive when is present alone under our experimental conditions, plays an important role when alloyed with Pd, increasing the catalytic activity of more than 50 % with respect to the monometallic Pd (from 541 to 836 h^{-1}). In terms of selectivity, contrary of what previously reported by Parvulescu and co-workers with SiO_2 imbedded bimetallic colloid, an increase in the content of Pd leads to higher production of HCAL up to 82 % in selectivity, with a consequential decrease in HCOH selectivity at isoconversion levels (Figure 12). As indicated by TEM and XPS analysis, these changes in selectivity are mainly caused by electronic interactions between the two alloyed metals, as suggested by XPS analysis, taking into account that the mean metal particle size is at similar range 2-3 nm.

3.7 Catalyst recycling

$Au_{50}Pd_{50}$/TiO_2 catalyst was finally tested in multiple consecutive reactions in order to evaluate its reusability. The results are reported in Figure 13. After the first run, the conversion decreased from 73 % to 50 % and it stabilised at a value of 45 % for the following runs. The selectivity, however, changed accordingly to the change in activity (HCOH decreased from 56 % to 45 %), meaning that the deactivation process affected mainly the catalytic activity. MP-AES analysis showed a significant loss of about 22 % of the Pd content after 4 runs that partially explain the loss in activity. Pd leaching was also detected when the reaction was performed with the monometallic Pd/TiO_2 catalyst, with a 28 % loss after 4 consecutive reactions. A control experiment using the filtrate solution without catalyst confirmed that eventual leached species do not take active part to the reaction. Another cause of activity loss could be a change in nanoparticle dimension; TEM analysis confirm this hypothesis, as an increase in the nanoparticles dimension as well as a broadening in size distribution was detected (Table 3). FTIR analysis was carried out on the fresh and used catalysts to study the presence/absence of adsorbed species before and after catalytic reaction. From the FTIR spectra collected on the fresh and used catalysts (Figure 14), it is possible to observe a weak band at 1670 cm^{-1} accompanied by a broad band in the range of 3700-3000 cm^{-1} that can be attributed to the OH stretching and bending typical for the stabilising agent used (PVA, Figure S15). However, the enhanced peak at 1670 cm^{-1} in the used catalyst can be also attributed to the alcoholic functional group of the CAL hydrogenation products and a series of small peaks at around 1500-1400 cm^{-1} typical account for the presence of aromatic C=C stretches

that indicate the presence of either COH or HCOH adsorbed on the surface of the catalyst (Figure S16). The stronger band at 3700-3000 cm^{-1} in the fresh catalyst is only due to remaining adsorbed water on the catalyst surface.
In order to improve the catalyst reusability, the $Au_{50}Pd_{50}/TiO_2$ catalyst was divided in 3 batches and heat treated at either 200, 300 or 400 °C as reported in the experimental section. High temperature reduction steps improve the metal-support interaction via a mechanism known as strong metal-support interaction (SMSI); [89] SMSI has been accounted for stability and selectivity improvement in several reaction due to the thin layer of TiO_x species that moves over and partially covers supported metal nanoparticles.[90–92] The results are reported in Table 3. Increasing the reduction temperature, the activity decreases from 73 to 50 % with the uncalcined and the 400 °C catalyst respectively. However, the stability improves considerably, with the $Au_{50}Pd_{50}/TiO_2$–300 and $Au_{50}Pd_{50}/TiO_2$–400 catalysts that do not loose activity even after 4 consecutive runs; only a small decrease in activity was reported for the $Au_{50}Pd_{50}/TiO_2$–200 catalyst (from 70 to 58 %). MP-AES tests on the final reaction solutions, revealed the absence of leached metal from the support, thus confirming that high temperature treatments help to stabilise the metal nanoparticles on the support surface. Moreover, XPS analysis don't reveal a significant change in surface metal composition with the heat treatment, so the change in activity correlated to a modification of the nanoparticles metal composition can be ruled out (Table S3). The overall loss in activity is probably due to both the suppressed hydrogen chemisorption due to the SMSI and the consequent increase in nanoparticles dimension with the increased reduction temperature, as reported in Table S4, with a measured average nanoparticle dimension that varies from 2.1 ± 0.6 nm to 5.3 ± 1.2 nm for the $Au_{50}Pd_{50}/TiO_2$ and $Au_{50}Pd_{50}/TiO_2$–400 catalysts respectively. On the other hand, the boost in stability due to the protective TiO_x surface layer prevent metal sintering phenomena during reaction, and this is confirmed again by TEM analysis (Figure S17): for high temperature treated catalysts, the nanoparticles dimension changes only slightly (from 5.3 ± 1.2 nm to 5.9 ± 1.3 nm for the $Au_{50}Pd_{50}/TiO_2$–400 catalyst). The SMSI effects not only the activity of the catalysts, but also the selectivity: increasing the reduction temperature, the selectivity towards CAL increases drastically from 40 to 83 % at iso-coversion, with $Au_{50}Pd_{50}/TiO_2$ and $Au_{50}Pd_{50}/TiO_2$–400 respectively. This is in clear contrast with many reports present in literature, where high temperature treated metal supported nanoparticles preferably reduce the C=O bond in α,β-unsaturated aldehydes.[33,72,87,93,94]

4. Conclusions

5. Captions for figures

Figure 1. Cinnamaldehyde hydrogenation pathways.

Figure 2. Representative images of the fresh catalysts (a) Au/TiO_2 (b) $Au_{95}Pd_5/TiO_2$ (c) $Au_{65}Pd_{35}/TiO_2$ (d) $Au_{50}Pd_{50}/TiO_2$ (e) $Au_{35}Pd_{65}/TiO_2$ (f) Pd/TiO_2.

Figure 3. Pd (3d) spectra for the Au_xPd_y/TiO_2 catalysts; nominal Au_xPd_y are indicated.

Figure 4. CO-DRIFT of (a) Pd/TiO_2, (b) $Au_{35}Pd_{65}/TiO_2$, (c) $Au_{50}Pd_{50}/TiO_2$, (d) $Au_{65}Pd_{35}/TiO_2$, (e) $Au_{95}Pd_5/TiO_2$ and (f) Au/TiO_2.

Figure 5. Pyridine-DRIFT of (a) $Au_{50}Pd_{50}/C$, (b) $Au_{50}Pd_{50}/MgO$, (c) $Au_{50}Pd_{50}/TiO_2$ and (d) $Au_{50}Pd_{50}/Fe_2O_3$.

Figure 6. Effect of (a) stirring speed (b) catalyst amount (c) H_2 pressure and (d) temperature on the TOF of the reaction.

Figure 7. Cinnamaldehyde hydrogenation profile. Reaction conditions 100 °C, 1 H_2 bar, catalyst amount 50 mg, CAL 4 mmol.

Figure 8. Adsorption mechanism for the CAL hydrogenation.

Figure 9. Solvent effect in the CAL hydrogenation. Reaction conditions 100 °C, 1 H_2 bar, catalyst amount 50 mg, CAL 4 mmol, substrate/metal molar ratio 1200:1.

Figure 10. Support effect in the CAL hydrogenation. Reaction conditions 100 °C, 1 H_2 bar, catalyst amount 50 mg, CAL 4 mmol, substrate/metal molar ratio 1200:1.

Figure 11. Au/Pd ratio effect in the CAL hydrogenation. Reaction conditions 100 °C, 1 H_2 bar, catalyst amount 50 mg, CAL 4 mmol, substrate/metal molar ratio 1200:1.

Figure 12. Au/Pd molar ratio effect in the CAL hydrogenation. Reaction conditions 100 °C, 1 H_2 bar, catalyst amount 50 mg, CAL 4 mmol, substrate/metal molar ratio 1200:1.

Figure 13. Reusability of the $Au_{50}Pd_{50}/TiO_2$ catalyst in the CAL hydrogenation. Reaction conditions 100 °C, 1 H_2 bar, catalyst amount 50 mg, CAL 4 mmol, substrate/metal molar ratio 1200:1.

Figure 14. FTIR analysis of the fresh and used catalyst.

6. Captions for tables

Table 1. Cinnamaldehyde hydrogenation activation energy for different catalysts.

Table 2. Hydrogenation of HCAL and COH. Reaction conditions 100 °C, 1 H_2 bar, catalyst amount 50 mg, CAL 4 mmol, substrate/metal molar ratio 1200:1.

Table 3. Catalysts reusability in the CAL hydrogenation. Reaction conditions 90 minutes, 100 °C, 1 H_2 bar, catalyst amount 50 mg, CAL 4 mmol, substrate/metal molar ratio 1200:1.

7. Figures

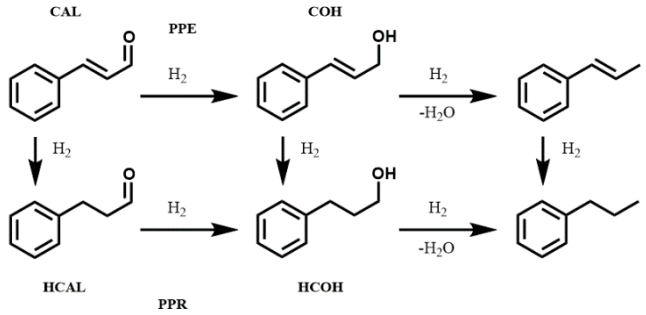

Figure 1

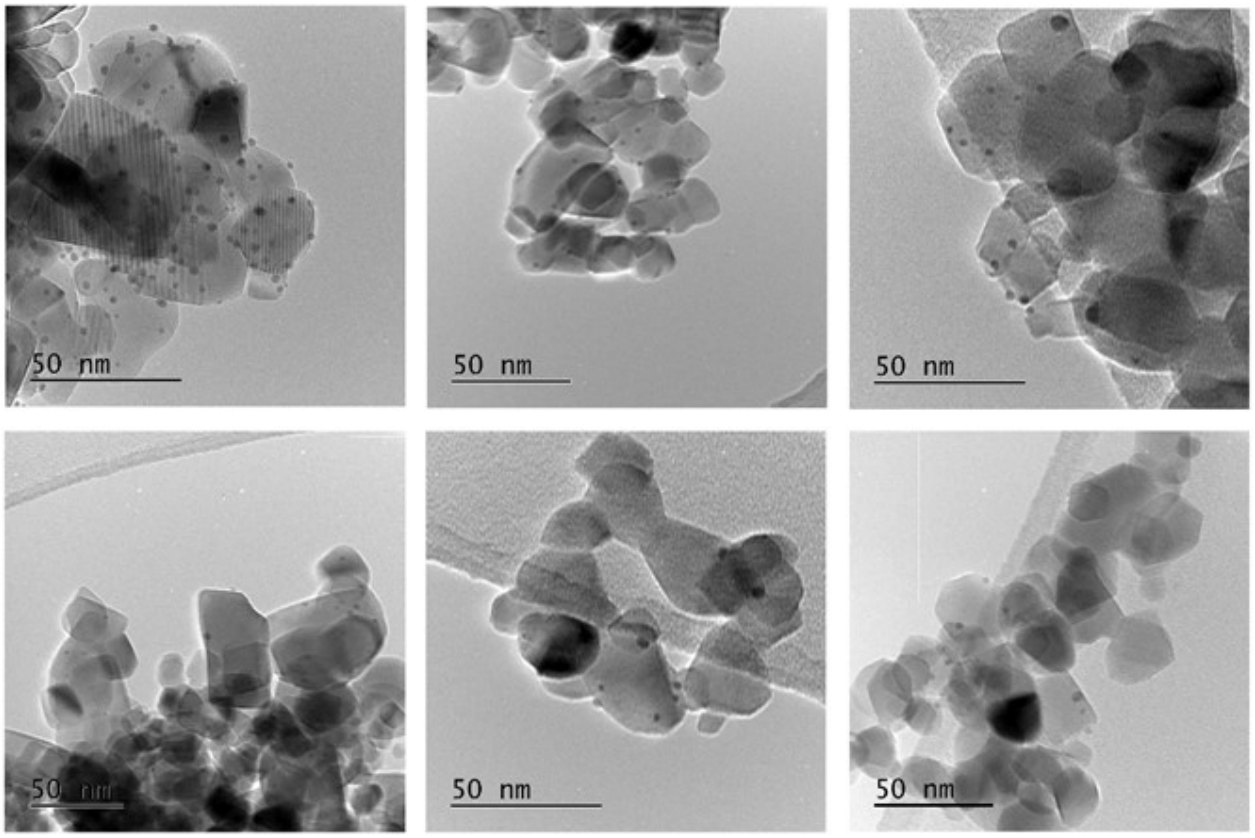

Figure 2

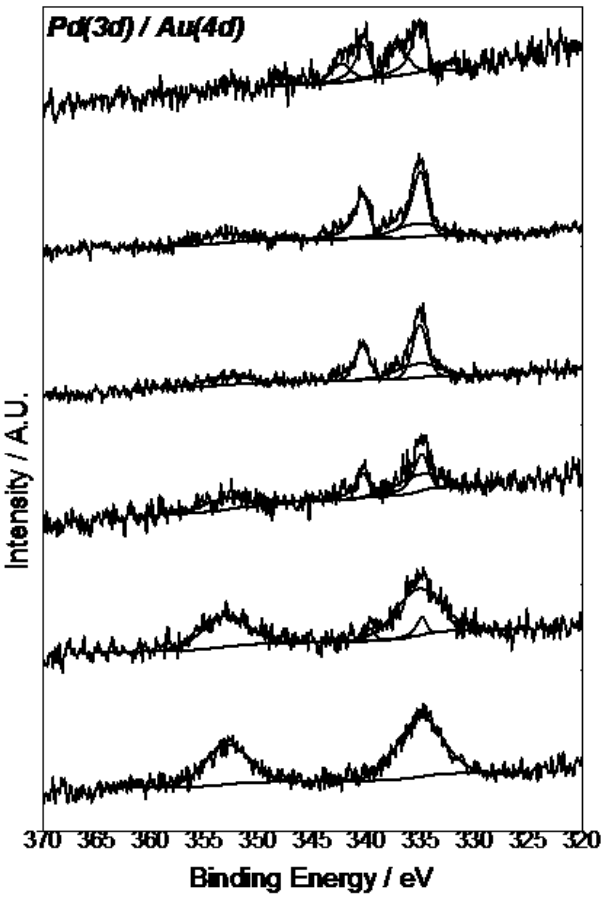

Figure 3

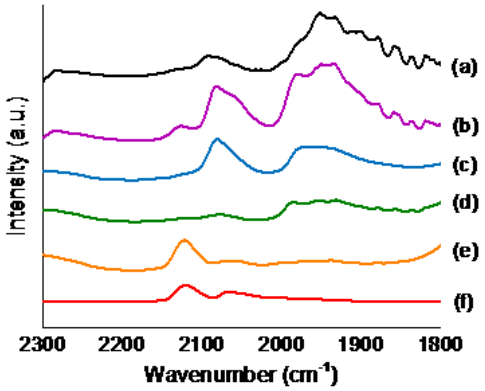

Figure 4

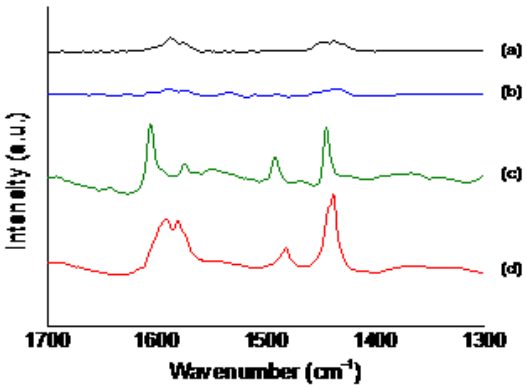
(a)
(b)
(c)
(d)
Intensity (a.u.)
1700
1600
1500
1400
1300
Wavenumber (cm-1)

Figure 5

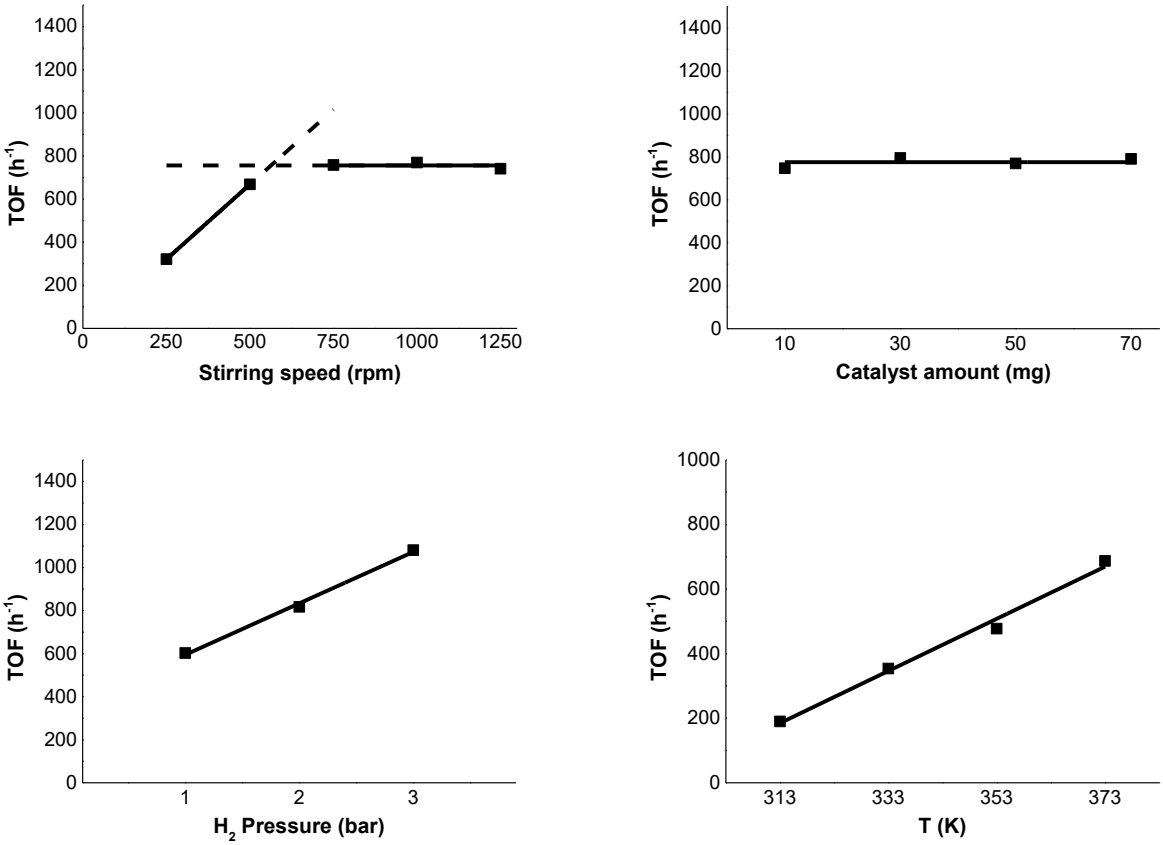
TOF (h-1)
Stirring speed (rpm)
Catalyst amount (mg)
H2 Pressure (bar)
T (K)

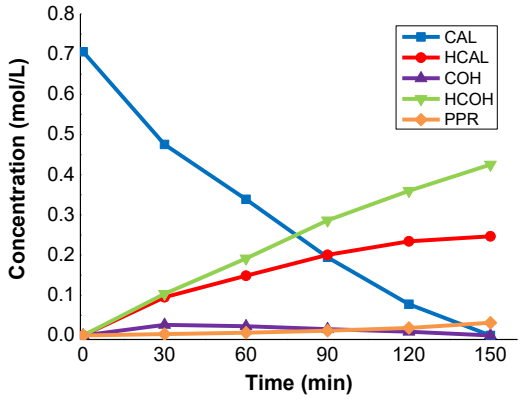

HCAL

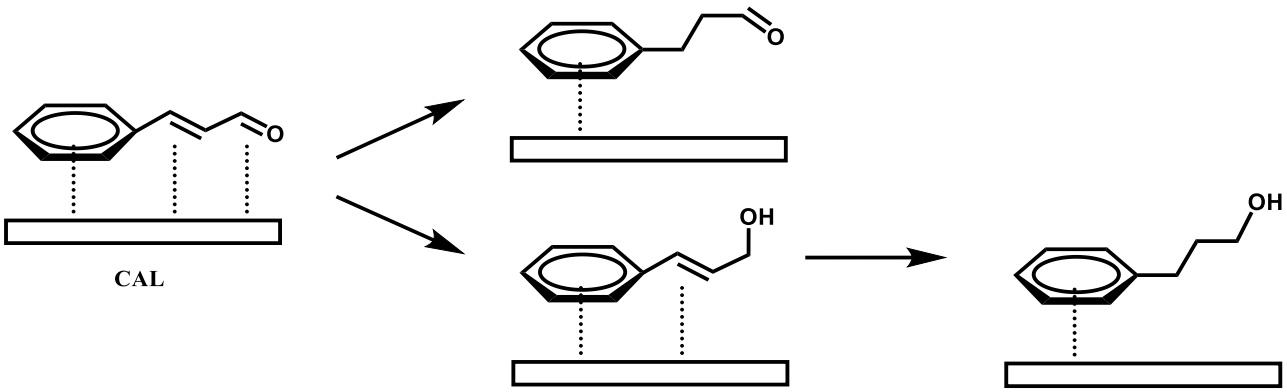

CAL COH HCOH

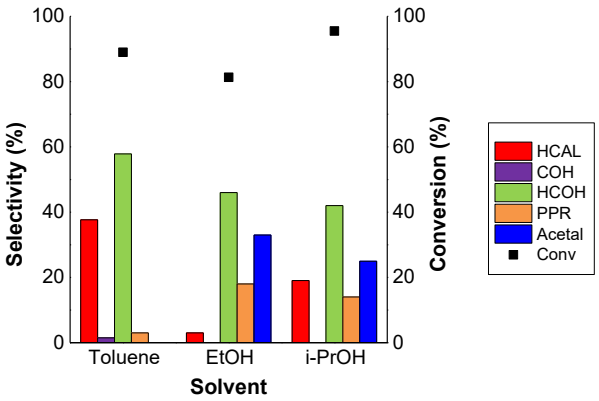

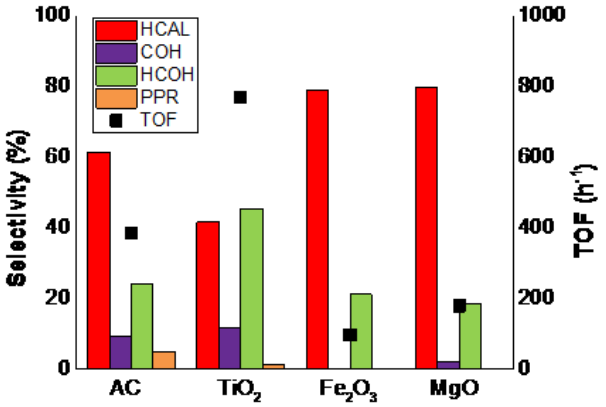
HCAL
COH
HCOH
PPR
TOF
Selectivity (%)
TOF (h-1)
100
80
60
40
20
0
1000
800
600
400
200
0
AC
TiO2
Fe2O3
MgO

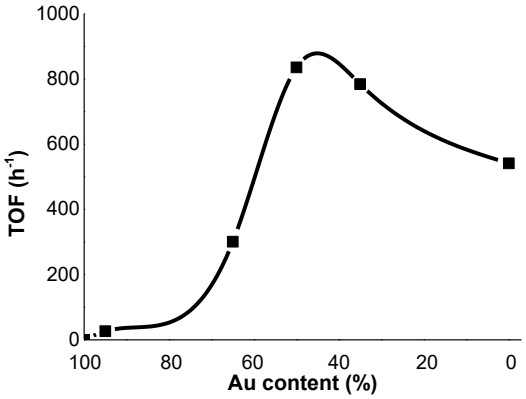
TOF (h-1)
1000
800
600
400
200
0
100
80
60
40
20
0
Au content (%)

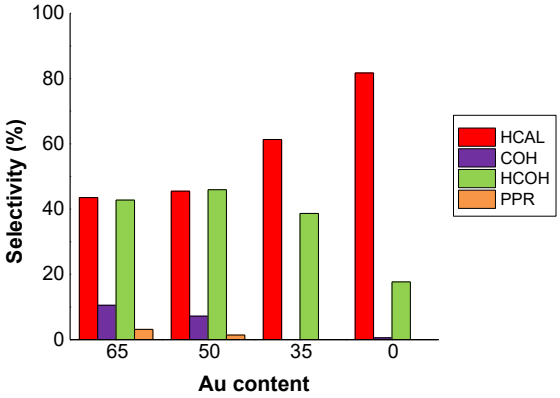
Selectivity (%)
100
80
60
40
20
0
65
50
35
0
Au content
HCAL
COH
HCOH
PPR

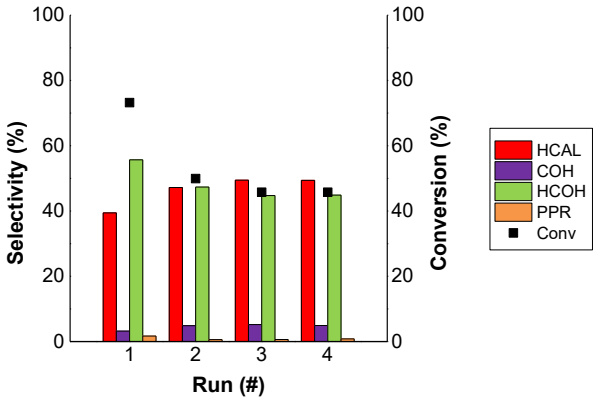

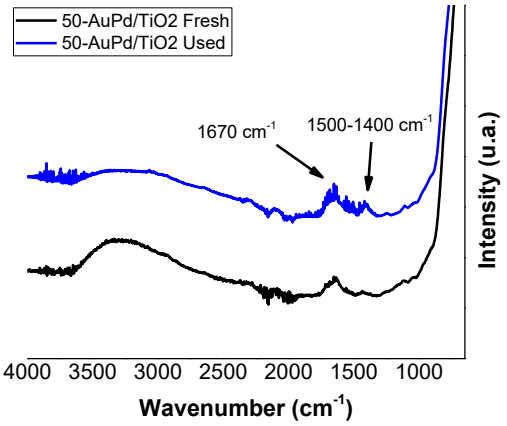

8. Tables

Table 1

Catalyst	Activation Energy (KJ/mol)	Ref.
5 % Pd/SiO_2	30.1	x
Co-B	18	x
Raney Co	35	
CoPt	17.3	x
5 % Ir/C	37	X
2 % Pt/SBA-15	21	x
2% Au/TiO_2	13	x
2% $Au/Pd/TiO_2$	37	
CoPt	17.3	x

Table 2

Substrate	Conv. (%)	Selectivity after 30 minutes of reaction	
		HCOH	PPR
HCAL	0	-	-
COH	100	92	8
CAL	35	46	1

Table 3

Catalyst	Run	Mean nanoparticles dimension (nm)	Conv. (%)	Selectivity after 90 minutes of reaction			
				HCAL	COH	HCOH	PPR
$Au_{50}Pd_{50}/TiO_2$	1	2.1 ± 0.6	73	39	3	56	2
$Au_{50}Pd_{50}/TiO_2$	4	3.3 ± 0.9	46	49	5	45	1
$Au_{50}Pd_{50}/TiO_2$ - 200	1	2.5 ± 0.8	70	66	0	33	1
$Au_{50}Pd_{50}/TiO_2$ - 200	4	3.4 ± 0.8	58	62	0	34	3
$Au_{50}Pd_{50}/TiO_2$ - 300	1	3.7 ± 1.0	56	81	0	18	2
$Au_{50}Pd_{50}/TiO_2$ - 300	4	3.8 ± 0.8	55	78	0	21	2
$Au_{50}Pd_{50}/TiO_2$ - 400	1	5.3 ± 1.2	50	83	0	16	1
$Au_{50}Pd_{50}/TiO_2$ - 400	4	5.9 ± 1.3	49	79	0	20	1

9. References

1 M. Haruta, T. Kobayashi, H. Sano and N. Yamada, *Chem. Lett.*, 1987, 405–408.
2 G. Hutchings, *J. Catal.*, 1985, **96**, 292–295.
3 A. Corma and P. Serna, *Science*, 2006, **313**, 332–4.
4 A. K. Sinha, S. Seelan, S. Tsubota and M. Haruta, *Angew. Chem. Int. Ed. Engl.*, 2004, **43**, 1546–8.
5 M. D. Hughes, Y.-J. Xu, P. Jenkins, P. McMorn, P. Landon, D. I. Enache, A. F. Carley, G. A. Attard, G. J. Hutchings, F. King, E. H. Stitt, P. Johnston, K. Griffin and C. J. Kiely, *Nature*, 2005, **437**, 1132–5.
6 A. Abad, P. Concepción, A. Corma and H. García, *Angew. Chem. Int. Ed. Engl.*, 2005, **44**, 4066–9.
7 A. Corma and H. Garcia, *Chem. Soc. Rev.*, 2008, **37**, 2096–126.
8 C. Della Pina, E. Falletta, L. Prati and M. Rossi, *Chem. Soc. Rev.*, 2008, **37**, 2077–2095.
9 J. K. Edwards and G. J. Hutchings, *Angew. Chem. Int. Ed. Engl.*, 2008, **47**, 9192–8.
10 A. Corma, R. Juárez, M. Boronat, F. Sánchez, M. Iglesias and H. García, *Chem. Commun. (Camb).*, 2011, **47**, 1446–1448.
11 D. McDonald and L. B. Hunt, *A Hystory of Platinum and its Allied Metals*, 1982.
12 S. E. Davis, M. S. Ide and R. J. Davis, *Green Chem.*, 2013, **15**, 17–45.
13 Z. Guo, B. Liu, Q. Zhang, W. Deng, Y. Wang and Y. Yang, *Chem. Soc. Rev.*, 2014, **43**, 3480–524.
14 J. Muzart, *Tetrahedron*, 2003, **59**, 5789–5816.
15 H.-J. Freund, N. Nilius, T. Risse and S. Schauermann, *Phys. Chem. Chem. Phys.*, 2014, **16**, 8148–8167.
16 G. C. Bond, *Metal-Catalysed Reactions of Hydrocarbons*, 2005.
17 L. Yin and J. Liebscher, *Chem. Rev.*, 2007, **107**, 133–173.
18 A. S. Roy, J. Mondal, B. Banerjee, P. Mondal, A. Bhaumik and S. M. Islam, *Appl. Catal. A Gen.*, 2014, **469**, 320–327.
19 B. Yuan, Y. Pan, Y. Li, B. Yin and H. Jiang, *Angew. Chemie - Int. Ed.*, 2010, **49**, 4054–4058.
20 D. I. Enache, J. K. Edwards, P. Landon, B. Solsona-Espriu, A. F. Carley, A. A. Herzing, M. Watanabe, C. J. Kiely, D. W. Knight and G. J. Hutchings, *Science (80-.).*, 2006, **311**, 362–365.
21 J. K. Edwards, B. Solsona, E. N. N, A. F. Carley, A. a Herzing, C. J. Kiely and G. J. Hutchings, *Science (80-.).*, 2009, **323**, 1037–1041.
22 J. K. Edwards and G. J. Hutchings, *Angew. Chemie Int. Ed.*, 2008, **47**, 9192–9198.
23 S. Mahmoud, A. Hammoudeh, S. Gharaibeh and J. Melsheimer, *J. Mol. Catal. A Chem.*, 2002, **178**, 161–167.
24 P. Mäki-Arvela, J. Hájek, T. Salmi and D. Y. Murzin, *Appl. Catal. A Gen.*, 2005, **292**, 1–49.
25 P. Gallezot and D. Richard, *Catal. Rev.*, 1998, **40**, 81–126.

26 L. A. Saudan, *Acc. Chem. Res.*, 2007, **40**, 1309–1319.
27 *Ullmann's Encyclopedia of Industrial Chemistry*, 7th edn., 2014.
28 US 4209643, 1978.
29 US 5632980 A, 1997.
30 E. Bus, R. Prins and J. a. van Bokhoven, *Catal. Commun.*, 2007, **8**, 1397–1402.
31 L. He, J. Ni, L. C. Wang, F. J. Yu, Y. Cao, H. Y. He and K. N. Fan, *Chem. - A Eur. J.*, 2009, **15**, 11833–11836.
32 H. Shi, N. Xu, D. Zhao and B.-Q. Xu, *Catal. Commun.*, 2008, **9**, 1949–1954.
33 C. Milone, C. Crisafulli, R. Ingoglia, L. Schipilliti and S. Galvagno, *Catal. Today*, 2007, **122**, 341–351.
34 X. Zhang, Y. C. Guo, Z. Cheng Zhang, J. Sen Gao and C. M. Xu, *J. Catal.*, 2012, **292**, 213–226.
35 C. Milone, M. C. Trapani and S. Galvagno, *Appl. Catal. A Gen.*, 2008, **337**, 163–167.
36 J. P. Tessonnier, L. Pesant, G. Ehret, M. J. Ledoux and C. Pham-Huu, *Appl. Catal. A Gen.*, 2005, **288**, 203–210.
37 A. M. R. Galletti, C. Antonetti, A. M. Venezia and G. Giambastiani, *Appl. Catal. A Gen.*, 2010, **386**, 124–131.
38 Y. Kume, K. Qiao, D. Tomida and C. Yokoyama, *Catal. Commun.*, 2008, **9**, 369–375.
39 K. Anderson, S. Cortiñas Fernández, C. Hardacre and P. C. Marr, *Inorg. Chem. Commun.*, 2004, **7**, 73–76.
40 Z. Tian, X. Xiang, L. Xie and F. Li, *Ind. Eng. Chem. Res. 2013,* 2013, **52**, 288−296.
41 S. Fujiwara, N. Takanashi, R. Nishiyabu and Y. Kubo, *Green Chem.*, 2014, 3230–3236.
42 M.-M. Wang, L. He, Y.-M. Liu, Y. Cao, H.-Y. He and K.-N. Fan, *Green Chem.*, 2011, **13**, 602.
43 P. Dash, N. A. Dehm and R. W. J. Scott, *J. Mol. Catal. A Chem.*, 2008, **286**, 114–119.
44 T. Szumełda, A. Drelinkiewicz, R. Kosydar and J. Gurgul, *Appl. Catal. A Gen.*, 2014, **487**, 1–15.
45 V. I. Pârvulescu, V. Pârvulescu, U. Endruschat, G. Filoti, F. E. Wagner, C. Kübel and R. Richards, *Chem. - A Eur. J.*, 2006, **12**, 2343–2357.
46 X. Yang, D. Chen, S. Liao, H. Song, Y. Li, Z. Fu and Y. Su, *J. Catal.*, 2012, **291**, 36–43.
47 H. Gu, X. Xu, A. A. Chen, P. Ao and X. Yan, *Catal. Commun.*, 2013, **41**, 65–69.
48 N. Dimitratos, J. A. Lopez-Sanchez, D. Morgan, A. F. Carley, R. Tiruvalam, C. J. Kiely, D. Bethell and G. J. Hutchings, *Phys. Chem. Chem. Phys.*, 2009, **11**, 5142–5153.
49 J. Feng, C. Ma, P. J. Miedziak, J. K. Edwards, G. L. Brett, D. Li, Y. Du, D. J. Morgan and G. J. Hutchings, *Dalt. Trans.*, 2013, **42**, 14498.
50 G. Zhan, Y. Hong, V. T. Mbah, J. Huang, A. R. Ibrahim, M. Du and Q. Li, *Appl. Catal. A Gen.*, 2012, **439**–**440**, 179–186.
51 D. Jin, X. Gu, X. Yu, G. Ding, H. Zhu and K. Yao, *Mater. Chem. Phys.*, 2008, **112**, 962–965.
52 Y. Lee and Y. Jeon, *J. korean Phys. Soc.*, 2000, **37**, 451–455.
53 M. Manzoli, A. Chiorino and F. Boccuzzi, *Surf. Sci.*, 2003, **532**–**535**, 377–382.
54 D. A. Panayotov, S. P. Burrows, J. T. Yates and J. R. Morris, *J. Phys. Chem. C*, 2011, **115**, 22400–22408.
55 M. Compagnoni, S. A. Kondrat, C. E. Chan-Thaw, D. J. Morgan, D. Wang, L. Prati, A. Villa, N. Dimitratos and I. Rossetti, *ChemCatChem*, 2016, **8**, 2136–2145.
56 K. Chakarova, M. Mihaylov, S. Ivanova, M. A. Centeno and K. Hadjiivanov, *J. Phys. Chem. C*, 2011, **115**, 21273–21282.
57 M. Mihaylov, H. Knözinger, K. Hadjiivanov and B. C. Gates, *Chemie-Ingenieur-Technik*, 2007, **79**, 795–806.
58 T. Tabakova, F. Boccuzzi, M. Manzoli and D. Andreeva, *Appl. Catal. A Gen.*, 2003, **252**, 385–397.
59 S. M. Rogers, C. R. A. Catlow, C. E. Chan-Thaw, D. Gianolio, E. K. Gibson, A. L. Gould, N. Jian, A. J. Logsdail, R. E. Palmer, L. Prati, N. Dimitratos, A. Villa and P. P. Wells, *ACS Catal.*, 2015, **5**, 4377–4384.
60 T. Lear, R. Marshall, J. A. Lopez-Sanchez, S. D. Jackson, T. M. Klapötke, M. Bäumer, G. Rupprechter, H. J. Freund and D. Lennon, *J. Chem. Phys.*, , DOI:10.1063/1.2101487.
61 H. Zhu, Z. Qin, W. Shan, W. Shen and J. Wang, *J. Catal.*, 2004, **225**, 267–277.
62 S. M. Rogers, C. R. A. Catlow, C. E. Chan-Thaw, A. Chutia, N. Jian, R. E. Palmer, M. Perdjon, A. Thetford, N. Dimitratos, A. Villa and P. P. Wells, *ACS Catal.*, 2017, acscatal.6b03190.
63 A. Villa, N. Dimitratos, C. E. Chan-Thaw, C. Hammond, G. M. Veith, D. Wang, M. Manzoli, L. Prati and G. J. Hutchings, *Chem. Soc. Rev.*, 2016, **45**, 4953–4994.
64 J. H. Carter, S. Althahban, E. Nowicka, S. J. Freakley, D. J. Morgan, P. M. Shah, S. Golunski, C. J. Kiely and G. J. Hutchings, *ACS Catal.*, 2016, **6**, 6623–6633.
65 F. Khairallah and A. Glisenti, *J. Mol. Catal. A Chem.*, 2007, **274**, 137–147.
66 X. Wang, S. Kim, C. Buda, M. Neurock, O. B. Koper and J. T. Yates, *J. Phys. Chem. C*, 2009, **113**, 2228–2234.
67 I. X. Green, C. Buda, Z. Zhang, M. Neurock and J. T. Yates, *J. Phys. Chem. C*, 2010, **114**, 16649–16659.
68 M. I. Zaki, M. a. Hasan, F. a. Al-Sagheer and L. Pasupulety, *Colloids Surfaces A Physicochem. Eng. Asp.*, 2001, **190**, 261–274.
69 V. V. Kumar, G. Naresh, M. Sudhakar, J. Tardio, S. K. Bhargava and A. Venugopal, *Appl. Catal. A Gen.*, 2015, **505**, 217–223.
70 G. a. M. Hussein, N. Sheppard, M. I. Zaki and R. B. Fahim, *J. Chem. Soc. Faraday Trans.*, 1989, **85**, 1723.
71 O. Fe, *Indian J. Chem.*, 2011, **50**, 1050–1055.
72 P. Mäki-Arvela, J. Hájek, T. Salmi and D. Y. Murzin, *Appl. Catal. A Gen.*, 2005, **292**, 1–49.
73 K. Q. Sun, Y. C. Hong, G. R. Zhang and B. Q. Xu, *ACS Catal.*, 2011, **1**, 1336–1346.
74 W. O. Oduro, N. Cailuo, K. M. K. Yu, H. Yang and S. C. Tsang, *Phys. Chem. Chem. Phys.*, 2011, **13**, 2590–602.
75 H. Li, X. Chen, M. Wang and Y. Xu, *Appl. Catal. A Gen.*, 2002, **225**, 117–130.

76 L. J. Durndell, C. M. a. Parlett, N. S. Hondow, M. a. Isaacs, K. Wilson and A. F. Lee, *Sci. Rep.*, 2015, **5**, 9425.
77 R. Liu, Y. Yu, K. Yoshida, G. Li, H. Jiang, M. Zhang, F. Zhao, S. ichiro Fujita and M. Arai, *J. Catal.*, 2010, **269**, 191–200.
78 H. Yamada and S. Goto, *J. Chem. Eng. Japan*, 2003, **36**, 586–589.
79 X. Zhang, H. Shi and B.-Q. Xu, *J. Catal.*, 2011, **279**, 75–87.
80 M. Okumura, T. Akita and M. Haruta, *Catal. Today*, 2002, **74**, 265–269.
81 M. Consonni, D. Jokic, D. Yu Murzin and R. Touroude, *J. Catal.*, 1999, **188**, 165–175.
82 C. Milone, M. L. Tropeano, G. Gulino, G. Neri, R. Ingoglia and S. Galvagno, *Chem. Comm.*, 2002, 868–869.
83 B. Bachiller-Baeza, I. Rodríguez-Ramos and A. Guerrero-Ruiz, *Appl. Catal. A Gen.*, 2001, **205**, 227–237.
84 P. Claus and C. Mohr, *J Am Chem Soc*, 2000, **122**, 11430–11439.
85 C. Milone, R. Ingoglia, M. L. Tropeano, G. Neri and S. Galvagno, *Chem. Commun.*, 2003, 868–869.
86 W. Gru, A. Bru, H. Hofmeister and P. Claus, *J. Phys. Chem. B*, 2004, 5709–5717.
87 M. Englisch, A. Jentys and J. A. Lercher, *J. Catal.*, 1997, **35**, 25–35.
88 S. Nishimura, N. Ikeda and K. Ebitani, *Catal. Today*, 2014, **232**, 89–98.
89 D. D. Eley, H. Pines and P. B. Weisz, *Advances in Catalysis*, 1989.
90 X. Feng, W. Li, D. Liu, Z. Zhang, Y. Duan and Y. Zhang, *Small*, 2017, 1700941.
91 J. C. Matsubu, S. Zhang, L. DeRita, N. S. Marinkovic, J. G. Chen, G. W. Graham, X. Pan and P. Christopher, *Nat. Chem.*, 2016, **9**, 120–127.
92 A. Kumar and V. Ramani, *ACS Catal.*, 2014, **4**, 1516–1525.
93 P. GALLEZOT and D. RICHARD, *Selective Hydrogenation of α,β-Unsaturated Aldehydes*, 1998, vol. 40.
94 A. A. Wismeijer, A. P. G. Kieboom and H. Van Bekkum, *Appl. Catal.*, 1986, **25**, 181–189.